Journal of Colloid and Interface Science 693 (2025) 137570

Contents lists available at ScienceDirect

Journal of Colloid And Interface Science

journal homepage: www.elsevier.com/locate/jcis

Regular Article

Nanoparticles do not influence droplet break-up, spreading, or splashing

Mete Abbot [a,1], Muhammad Hamza Iqbal [b,1], Lingyue Liu [c], Erin Koos [c], Ilia V. Roisman [a], Jeanette Hussong [a], Alfonso Arturo Castrejón-Pita [d], José Rafael Castrejón-Pita [b,*]

[a] Institute for Fluid Mechanics and Aerodynamics, Technical University of Darmstadt, Alarich-Weiss-Straße 10, Darmstadt, 64287, Germany
[b] Department of Mechanical Engineering, University College London, London, WC1E 7JE, United Kingdom
[c] Department of Chemical Engineering, KU Leuven, Leuven, 3001, Belgium
[d] Department of Engineering Science, University of Oxford, Oxford, OX1 3PJ, United Kingdom

GRAPHICAL ABSTRACT

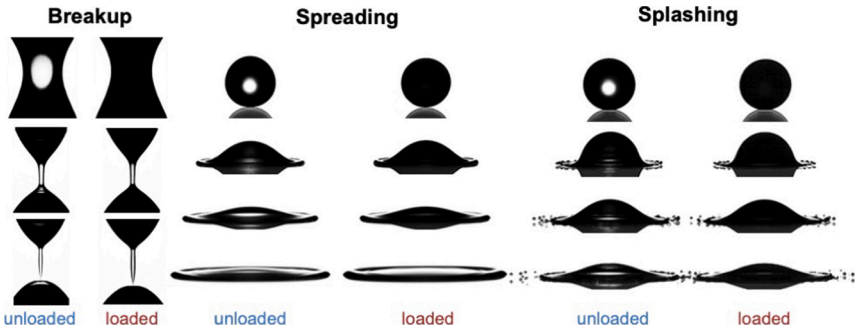

ARTICLE INFO

Keywords:
Nanoparticles
Drop impact
Droplet
Breakup
Spreading
Splashing

ABSTRACT

The dynamics of nanoparticle-laden droplets, from dripping to impact, have remained a subject of intense debate due to conflicting reports in the literature. Here, we address this controversy by systematically investigating the breakup, impact, spreading, and splashing behavior of fully characterized additive-free silica nanosuspensions synthesized via the Stöber process. In the absence of additives, we find that nanoparticles exert negligible influence on the fluid viscosity and dynamic behavior of droplets during break up, spreading, and splashing — even in suspensions with a high loading concentration (15 wt.%). This work highlights the pivotal role of additives, dispersants, and interparticle interactions in governing droplet behavior. Our findings offer crucial insights for a wide range of fields, including inkjet printing and spray coating.

1. Introduction

The journey of a liquid droplet, from formation to impact on a surface, encapsulates a complex interplay between interfacial forces and inner dynamics [1–3]. This odyssey begins with the droplet dripping off a tap or nozzle, and continues as the droplet grows under a delicate balance between surface tension, inertial, gravitational, and viscous forces, then breaking up and falling toward a substrate [4,5]. Upon im-

* Corresponding author.
E-mail address: r.pita@ucl.ac.uk (J.R. Castrejón-Pita).
[1] These authors contributed equally to this work.

https://doi.org/10.1016/j.jcis.2025.137570
Received 30 January 2025; Received in revised form 17 March 2025; Accepted 10 April 2025
Available online 16 April 2025

pact, where the interplay between capillary forces, wetting properties, gas viscosity, and kinetics (among other possible factors) determines the outcome: smooth spreading or dramatic fragmentation into a myriad of secondary droplets, a phenomenon known as splashing [6,7].

Extensive research on simple (Newtonian) fluids has identified how fluid properties, such as density, viscosity, surface tension, as well as gas viscosity, substrate wetting properties, and morphology, influence droplet breakup and splashing [6]. However, most real-world and industrial fluids contain micro- and nanoscale particles, and other additives, that may alter the fluid behavior [8,9]. There is a strong industrial impetus to develop nanosuspension droplets with high particle weight fractions. For instance, in coating applications, a high particle loading suspension requires fewer passes to achieve the desired film thickness [10,11]. In printing, dilute suspensions can lead to excessive substrate wetting, prolonged drying times, and increased energy consumption [12]. Understanding how particle loading affects the dynamics of breakup, impact, spreading, and splashing is critical for applications ranging from inkjet printing [13] and spray cooling [14,15] to drug delivery [16] and agriculture [17]. However, conflicting evidence in experiments, and theoretical and numerical models, have clouded our understanding of the nanoparticle (NP) influence on droplet dynamics.

The study of liquid thinning and breakup presents theoretical challenges marked by the presence of finite-time singularities and discrepancies between length and time scales within the Navier-Stokes equation [18,19]. Experiments are equally demanding, necessitating the observation of features across various sizes and temporal scales [19,20]. Nevertheless, past works have shown that the thinning neck during the pinch off of inviscid fluids scales as $r/R \sim \tau^{2/3}$, with the shape of the breakup region exhibiting a self-similarity angle of 18.1 degrees [21,22]; here the time τ is made dimensionless by the capillary time $t_c = \sqrt{\rho R^3/\sigma}$, with σ and ρ being the liquid surface tension and density respectively, r is the necking radius, and R is a characteristic size, typically the nozzle radius. For near-inviscid liquids, e.g. water or ethanol, viscosity effects only begin to influence the pinch-off dynamics at neck diameters around $r \approx 6$ nm, or when the neck size approaches $r/R \propto Oh^2$, here Oh is the Ohnesorge number $Oh = \frac{\eta}{\sqrt{2\rho R\sigma}}$, where η is the viscosity [19]. These scales cannot be observed by conventional means so viscosity effects are considered negligible in these liquids. Other works have found that the addition of micro- or nanoparticles influences droplet stretching and breakup, transitioning from a bulk-dominated flow to a local particle-concentration-dominated regime near the pinch-off [23–26]. The particle concentration affects the dynamics, with Newtonian-like behavior seen at low concentrations, while denser colloids and certain nanoparticles exhibit thinning, thickening, or strain hardening [27–29]. Additionally, nanoparticle stiffness and non-spherical nanomaterials further influence the extensional behavior [30–32]. Regardless of their industrial importance, nanosuspensions are inherently unstable due to the nanoparticles' natural high surface energy, which drives them to aggregate and settle out of suspension [33]. Surfactants [34], salts [35], pH modifiers [36], and polymers [37] are often incorporated to counteract aggregation and stabilize the suspension; additives create inter-particle repulsive forces, or steric barriers, preventing aggregation and ensuring long-term stability. Unfortunately, additives bring undesired, and often unknown, effects such as increased viscosity and changes in the flow properties [38].

In contrast to conventional suspensions, the Stöber process produces monodisperse silica nanoparticles with a hydrophilic surface rich in silanol groups [39]. These groups form strong hydrogen bonds with water, creating a robust hydration layer that effectively prevents particle aggregation. Resulting Stöber nanosuspensions exhibit remarkable stability without the need for stabilizers or additives, simplifying their formulation and reducing potential undesired rheological effects. Thus the main advantage of this process is the production of clean, monodisperse, and spherical particles with controllable size [40]. Regrettably, the additive-free Stöber process remains limited to small-scale laboratory production, and thus the vast majority of commercially available nanosuspensions contain stabilizing additives. Nevertheless, the process remains as one of the most widely used wet chemistry synthetic approaches to silica nanoparticles. Possible disadvantages of the Stöber process are that its main solvent is alcohol, and thus requires special handling limiting scalability. In addition, Stöber nanoparticles need to be washed multiple times to replace the base liquid, the particle size is strongly dependent on the concentrations of reagents and temperature, and the cost of precursors, such as tetraethoxysilane, is high [41].

As observed by widely used techniques such as CaBER [42] and TriMaster [43], the stretching behavior of additive-loaded suspensions change depending on factors such as the particle type, size, shape, roundness, roughness, and particle concentration. Past works on filament stretching have found that particles in a solution lead to uneven bridge shape and faster breakup [23]. Interestingly, it has also been discovered that for fast stretching, particles move away from the narrowing area producing a low-viscosity localized region that evolves as if no particles were present. This faster breakup has been successfully modeled in terms of particle size and concentration using one-dimensional models [25]. Other works present a mixed picture, with some studies suggesting that, at very low concentrations, suspensions of spherical nanoparticles behave similarly to Newtonian fluids during stretching [27]. However, denser suspensions of relatively large nanoparticles (100-700 nm) exhibit Newtonian behavior at low stretching speeds but show thickening and ultimately a solid-like fracture at higher speeds [28]. The influence of nanoparticles on fluid stretching is further complicated by observations of strain-hardening behavior in polymer solutions suggesting that other factors, beyond simple particle size and concentration, are at play [29]. One possibility is that particle clustering leads to the formation of aggregates, with the resulting structures having a complex shape and a larger size, similar to microsuspensions. Intriguingly, studies on ferrofluids reveal that the application of a magnetic field can enhance extensional viscosity and increase breakup time, especially at higher magnetic nanoparticle concentrations [27,44]. For larger micron-sized magnetic particles this effect has also been observed highlighting the role of particle-particle interactions on the fluid's rheological properties [45]. Particle-particle interaction are mainly affected by the electrostatic stabilizing, and the hydration layers. For the case of silica nanoparticles, a strong electrical double layer is known to exist, up to a volume fraction of 0.3, leading to strong electrostatic repulsion and higher stability. This behavior is also seen at higher shear rates [14,46]. On the other hand, the increase of the effective viscosity of the magnetorheological liquids has been associated with chain formation along the magnetic flux, driven by induction. This further proves that particle interactions and networks are factors that modify the thinning behavior. Studies with rod-like soft nanoparticles have shown that increased flexibility leads to higher extensional viscosity due to the formation of hairpin-like structures within the flow [30], concluding that stiffness also plays a crucial role on the extensional behavior, and thus in the breakup.

Other studies have found that nanoparticles in unstable solutions, e.g. carbon nanotubes (CNTs) and graphene oxide, can arrange themselves into long deformable structures bringing changes to the extensional behavior [47]. Suspensions with pretreated CNTs are known to exhibit enhanced extensional viscosity due to structural alignment in the flow direction, while untreated CNTs cause irregularities in the liquid bridge and an abrupt breakup [31]. On the other hand, the stretching of graphene oxide suspensions displays a strong dependence on initial conditions, with graphene oxide flakes migrating away from the necking region during stretching [32]. While these findings highlight the impact of complex nanoparticles on the extensional properties, the effects of stable, smooth, round, and well-dispersed nanoparticles in the dynamics of additive-free systems were yet to be studied.

Having covered some of the factors governing extensional properties and droplet formation of nanosuspensions, we now turn our attention to the dynamics of droplet impact, spreading, and splashing. Liquid droplets impacting solid surfaces underpin a vast array of both natu-

ral and industrial phenomena. The outcomes of droplet impact, namely spreading (smooth deposition) and splashing [1], have been pivotal in driving innovations in fields ranging from agriculture to inkjet printing and forensic science. Extensive studies with pure liquids have focused on the role of surface roughness [48], substrate stiffness [49], wettability [50], surfactants [51], and polymer additives [52], on the impact dynamics [53,54], but the study of nanoparticle suspensions remains limited with conflicting results.

Recent studies have revealed that nanoparticle characteristics – such as size, concentration, and wettability – strongly influence the spreading behavior on smooth solid surfaces [55–64]. In fact, a minimal addition of nanoparticles can significantly alter wetting properties, with smaller nanoparticles producing more pronounced contact angle changes as concentration increases [55]. In contrast, studies on large nanoparticles show that the contact angle increases with particle size [56]. Investigations into various water-based nanofluids of Al_2O_3, TiO_2, and Cu nanoparticles have revealed that irrespective of particle type, or concentration, nanoparticles consistently increase contact angles compared to pure water [57]. For hydrophilic nanoparticles, the effects on spreading are negligible, while hydrophobic particles promote contact line pinning, often due to nanoparticle positioning at the three-phase contact line [58]. A contrasting study suggests that hydrophilic nanoparticles inhibit dynamic wetting, and is likely due to increased viscosity [59]. Widening the scope of nanofluid research, a study on vibration-triggered spreading revealed that low concentrations (0.001 volume fraction) of 150 nm SiO_2 nanoparticles induce a distinctly different spreading regime compared to water, with nanofluid droplets flattening and spreading rapidly under vibration while water droplets maintain a stable shape [60].

The effect of nanoparticles has also been studied at the transition from spreading to splashing. Recent work has found that tetradecane droplets with 10 nm silver nanoparticles spread, without splashing, at low-impact velocities, similar to Newtonian fluids. Intriguingly, as velocities increase, and pass the splashing threshold, a second velocity threshold is found beyond the point in which splashing is suppressed. This phenomenon contradicts Newtonian behavior, where splash suppression has been attributed to nanoscopic interactions and unobserved non-Newtonian behavior, such as shear-thickening at very high shear rates, which are not detectable by conventional rheological measurements [61]. A contrasting study examined the influence of nanoparticles on splashing using commercial Al_2O_3-water nanofluids on smooth surfaces. Remarkably, it was observed that nanoparticles, as small as 45 nm in diameter and at concentrations as low as 0.01 wt.%, could promote splashing at lower velocities than those required for the base liquids alone. This earlier splashing is attributed to the faster expansion of the lamella and an increase of the stresses in the thin gas layer beneath [62,63]. In contradiction to this work, other studies have found that low concentrations of 15 nm silver nanoparticles significantly reduce both the spreading and receding velocities of droplets [64]. The conflicting results across all these studies may stem from a lack of a detailed suspension characterization at the appropriate time scales [61], i.e. the existence of undesirable high-speed rheological and dynamic wetting effects, brought by the use of off-the-shelf commercial nanoparticles, surfactants, additives, stabilizers, and pH buffers [55,57–59,61–65].

Indeed, particle-laden fluids exhibit distinct flow regimes based on the shear rate. At low shear rates, particle motion is governed by Brownian diffusion, producing a Newtonian flow. As shear rates rise, particles align with the flow streamlines in a hydrodynamic regime. The transition from a diffusion-dominated regime to a flow-dominated hydrodynamic regime is quantified by the Péclet condition, i.e. $Pe \geq 1$, which compares the effects of fluid flow to random particle motion, here $Pe = \frac{6\pi\eta\dot{\gamma}(\frac{D_p}{2})^3}{k_B T}$, $\dot{\gamma}$ is the shear rate, D_p the particle diameter, k_B is the Boltzmann constant, and T the temperature. For most nanofluids, this diffusion to hydrodynamic transition occurs at impact velocities $U_0 = \dot{\gamma} D_0 = \mathcal{O}(1 - 10^3)$ m/s, where D_0 is the initial drop diameter. See Supplementary Material Notes 1 and 2 for further details.

Once in the hydrodynamic regime ($Pe \gg 1$), the ability of particles to follow the fluid streamlines is quantified by the Stokes number $St = \frac{\rho_p D_p^2}{18\eta}\dot{\gamma}$, where ρ_p is the density of the particle [62]. In systems where $St \gg 1$, at very high shear rates, particles detach from the flow, leading to a non-linear relationship between shear stress and shear rate, which is characteristic of non-Newtonian fluids. In most nanofluids, this transition occurs at very high impact velocities, $U_0 = \mathcal{O}(10^6 - 10^8)$ m/s. Hence, for the range of conditions covered by most past experiments, nanoparticles are either in diffusion-dominated transport or near-perfect advective transport, which lead to Newtonian behavior. A lack of Newtonian behavior in nanosuspension should thus be the result of other effects, such as to the presence of additives, strong interparticle interactions, strong surface activity, particle-substrate interactions, or the lack of suspension stability which leads to aggregation and effective particle sizes beyond the nanoscale.

Previous studies have claimed that nanoparticles themselves significantly alter droplet dynamics, i.e. liquid break-up [23,25,27–32,44,45,47], wetting [55–60], spreading [55–64], and splashing [61–63]. These studies represent essential steps in understanding nanosuspension behavior, but many of them use commercial suspensions, which typically include additives such as surfactants, pH and salinity modifiers, and/or polymer stabilizers. The independent effects of each of these additives, as well as the particles, on droplet dynamics have yet to be demonstrated. In other words, it is unknown whether additives have undesired effects on the dynamics of colloidal liquids.

Colloidal characterization is also complicated. The stability of dispersions is usually assessed by the Zeta potential, but highly loaded suspensions are often characterized by extrapolating the Zeta potential of dilute solutions to higher concentrations, this without a rigorous validation. In addition, particle sphericity and surface smoothness are also not often meticulously tested or reported. Other issues affecting experiments include the scarcity of information on surface cleaning and experimental repeatability. Furthermore, nozzle and needle tip cleaning and replacement in drop generation is essential, as particle adsorption at the interface (after repeated) use can lead to clogging, which can artificially modify particle concentration.

In this study, we employ additive-free particles synthesized in-house. We have followed a strict protocol that ensures that both the substrate and the needle tip are replaced after each breakup and impact event. Our data is the result of at least 3 separate events. In terms of experimental control, we minimized the exposure of imaging light (heat) to less than 20 seconds per experiment to mitigate potential heating effects. In addition, we have validated stability across both low and high concentrations and confirmed particle sphericity and surface smoothness through electron and atomic force microscopy. Our experimental results demonstrate that nanoparticles do not influence droplet behavior throughout its journey from break up to impact. Our results highlight the often overlooked role of additives, surfactants, and inter-particle interactions on droplet dynamics.

2. Experimental details

2.1. Overview of the experiments

In our experiments, droplets were created by slowly pumping fluid, using a syringe pump, through a vertically oriented long blunt nozzle. The experimental setup is shown in Fig. 1a. In brief, our experiments consisted of recording the dynamics of droplets at two points: at the nozzle during dripping to capture the thinning, necking, and breakup, and at the impact point on a smooth glass solid surface to visualize spreading and splashing. The impacting speed was adjusted by varying the distance from the nozzle to the impact surface. Ultra high-speed imaging and image analysis were used to extract thinning diameters,

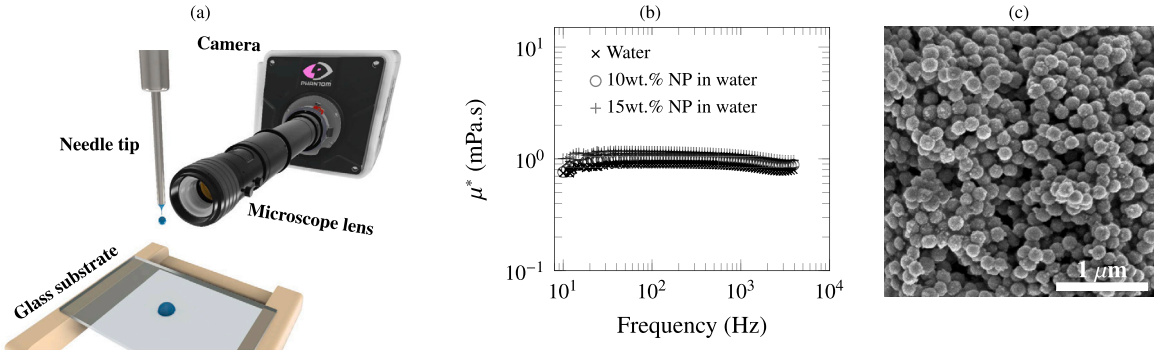

Fig. 1. (a) Experimental setup used to capture the necking during dripping and the impact of the drop on the glass substrate. (b) Viscosity measured by a PAV rheometer as a function of frequency, revealing a negligible impact of nanoparticles on fluid behavior across a range of frequencies. (c) SEM image confirming the spherical morphology and uniform size distribution of silica nanoparticles used in this study.

Table 1
Physical properties of liquid samples, including viscosity (η), density (ρ), and surface tension (σ) at temperature T = 20 ± 1.0 Celsius.

Sample Name	W:E	Water wt.%	Ethanol wt.%	NP wt.%	η ±0.2 mPa s	ρ ±0.2 kg/m^3	σ ±0.5 mN/m
Water	1:0	100	0	0	0.9	997.0	72.4
5% NP in Water	1:0	95	0	5	1.0	1024.5	72.3
10% NP in Water	1:0	90	0	10	1.0	1053.5	72.2
15% NP in Water	1:0	85	0	15	1.0	1084.2	72.0
Ethanol	0:1	0	100	0	1.2	789.3	22.4
5% NP in Ethanol	0:1	0	95	5	1.2	814.8	22.4
10% NP in Ethanol	0:1	0	90	10	1.2	842.3	22.5
15% NP in Ethanol	0:1	0	85	15	1.3	871.8	22.4
75% Ethanol	1:3	25	75	0	2.1	832.9	24.9
10% NP in 75% Ethanol	1:3	23	67	10	2.2	887.7	25.1
50% Ethanol	1:1	50	50	0	2.8	882.1	28.5
10% NP in 50% Ethanol	1:1	45	45	10	2.8	937.5	28.5
25% Ethanol	3:1	75	25	0	2.4	937.3	36.0
10% NP in 25% Ethanol	3:1	68	22	10	2.4	993.4	36.0

impact, and contact line speeds, spreading diameters, and the dynamic contact angle. Our results contrast the behavior between the base liquids and the nanosuspension. Water and ethanol solutions were used as base fluids in this work. The nanoparticle suspensions were characterized by high-frequency Piezo Axial Vibrator (PAV) rheometry, with results demonstrating a minimal effect of the particles on the resulting liquid's viscosity, with a value of $\eta^* \approx 1.0 \pm 0.2$ mPa s, as seen in Fig. 1b. The PAV complex viscosity is used to calculate the shear viscosity assuming the validity of the Cox-Mertz rule for our non-structuring suspensions. These values align with Einstein's classic equation, which predicts the viscosity of dilute suspensions of non-interacting solid spheres, $\eta_s = \eta_0(1 + \frac{5}{2}\phi)$, where η_s is the overall viscosity of the suspension, η_0 is the viscosity of the liquid without nanoparticles, and ϕ is the volume fraction of nanoparticles in the liquid. Even at the highest concentration of nanoparticles, (15 wt.%, corresponding to a volume fraction of 0.06 in ethanol and 0.076 in water), the measured viscosity closely matches the values predicted by Einstein's equation: 1.33 mPa s in ethanol and 1.19 mPa s in water. While nanoparticles typically have complex interactions leading to high viscosities, the agreement of our measurements with Einstein's equation implies that our nanoparticles behave like well-dispersed non-interacting solid spheres. Particle size and shape are shown in Fig. 1c as part of an SEM image. The Stöber particle hydrophilicity guarantees a minimal effect on surface tension, with the measured suspension surface tension staying within the error (less than ± 0.3 mN/m) of that of the base liquid. Both the dynamics light scattering (DLS) and atomic force microscopy (AFM) confirm a particle size of 152.5 ± 11.8 nm with a polydispersity index of 0.11. Zeta potentials, quantifying both the electrostatic potential at the particle shear plane and the suspension stability, were measured to be -45.13 ± 1.48 mV for water suspensions and -33.40 ± 0.65 mV for ethanol, confirming their inherent stability. Water and ethanol nanosuspensions of up to a concentration of 15 wt.% (weight) were used; with the particle concentration limit only reached by the clustering of the suspension. For our ethanol-based nanosuspensions, the transition to a flow-dominated hydrodynamic regime occurs at $U_0 \geq 1.1$ m/s while hydrodynamic particle detachment happens at an impact velocity of $U_0 = \dot{\gamma} D_0 \geq 1.1 \times 10^6$ m/s. Therefore, our conditions correspond to a near-perfect advective transport. Our experiments were carried out in the domain: $0.005 < Oh < 0.009$. A list of the samples along with the relevant physical properties is presented in Table 1.

2.2. Nanoparticle synthesis

In this work, the Stöber process was used to produce spherical, smooth, and well-dispersed silica nanoparticles with clean surfaces. During formulation, a 4.54 ml ammonium hydroxide solution (28-30%, Sigma-Aldrich), 87.39 ml of anhydrous ethanol (99.8%, Fischer Chemical), and 3.6 ml of ultrapure water (Arium 611DI, Sartorius Stedim Biotech) were first mixed in a 250 ml round bottom flask with a PTFE stir bar for 10 min. Subsequently, 4.47 ml of tetraethyl orthosilicate (TEOS, 98%, Acros Organics) were gradually added using a syringe pump (PHD 4400 Hpsi, Harvard Apparatus) at a flow rate of 500 μl/h. The reaction mixture was left overnight to ensure a complete reaction. The resulting turbid suspensions were centrifuged at 16 Celsius using an Avanti J-30I Centrifuge (Beckman) at 9000 rpm for 30 min. The supernatant was discarded, and the nanoparticles were redispersed in anhydrous ethanol using an ultrasound bath for 30 minutes. The suspensions were centrifuged again, and the supernatant was removed, completing the

first washing step. This washing process was repeated three times to ensure pristine silica surfaces. Finally, the nanoparticles were dispersed in anhydrous ethanol, according to the desired volume fraction. For water-based suspensions, the anhydrous ethanol from the last two washing cycles was replaced with ultrapure water. The final samples were then diluted with the base liquid, water, or/and ethanol, to form suspensions at the desired concentrations.

2.3. Nanoparticle and nanosuspension characterization

The equilibrium surface tension of the suspensions was measured using a pendant-drop tensiometer (Attension, Biolin Scientific) at room temperature (20.0 ± 1.0 Celsius) with a frame rate of 14 FPS over 30 s duration. The observed value for each sample remained constant throughout the experiment, independent of the droplet sizes. The error on the surface tension was less than ± 0.2 mN/m.

The nanoparticle suspensions were characterized using a commercial 3D Dynamic Light Scattering device - 3D DLS (from LS Instruments); the average particle size obtained was of 152.0 ± 11.9 nm. The temperature was constant throughout the experiments, at 20.0 ± 1.0 Celsius. The results were averaged using three different tests on three identical samples.

A TriPAV (Trijet Limited, Cambridge, UK) Piezo Axial Vibrator - PAV rheometer was used to characterize the high-frequency rheology of the suspensions under squeeze flow conditions. The frequency sweep was performed up to 5,000 Hz as recommended by the manufacturer. The lower plate excitation is driven by an external Lock-in amplifier with an exciting voltage of 5 V which results in a maximum displacement of around 50 nm, ensuring a strain below 0.2% for a liquid gap height of 17.67 μm. The PAV measurements were performed at a temperature of 20 ± 1.0 Celsius; the final result is the average of three repeating sweeps on three identical samples. The experimental error associated to the PAV viscosity measurement is less than ± 0.2 mPa s.

2.4. Droplet generation and imaging

Droplets were generated using an AL 300 Aladdin InfusionONE Syringe Pump (World Precision Instruments GmbH, Germany) operating under the constant flow rate mode to ensure precise control over the liquid flow. A stainless steel blunt-end dispensing tip (gauge 18 with an inner diameter of 0.83 mm) was securely attached to the syringe by nylon tubing, and vertically aligned using a calibrated level. This configuration facilitated pendant droplet formation and subsequent detachment under gravity. The pump speed was carefully maintained at 10 μl/min to minimize the risk of nanoparticle agglomeration within the dispensing tip. This pumping rate ensured that each droplet formed consistently over approximately 10 seconds, thereby promoting stable droplet formation and uniform nanoparticle distribution within each droplet. Under these conditions, droplets were produced in the range from $D_0 = 2.45$ mm (for the 15 wt.% NP in ethanol) to 2.67 mm (for the 25 wt.% ethanol). The dispensing tip was affixed to a precision mechanical vertical stage to adjust the height, enabling precise control over the droplet's impact velocity which was varied in the range from $U_0 = 1.00$ m/s for smooth spreading to 2.37 m/s for splashing events. Each experiment was repeated at least 3 times. After each experiment, a clean new solid flat glass substrate (microscope slides) was used to ensure reproducibility and minimize surface contamination. This practice prevented the accumulation of nanoparticles on the glass substrate. We performed AFM imaging, as seen in Supplementary Material Fig. S1b, to confirm that even rigorous cleaning could leave residual nanoparticles on the substrate.

The droplet formation and breakup imaging was performed using a Phantom TMX5010 ultra high-speed camera equipped with a 12× Navitar microscope lens. The camera was positioned to capture a side view, under a shadowgraph mode, at a spatial resolution of 133 pixels/mm at a field of view of 1280 x 256 pixels. The frame rate was adjusted to 150,000 frames per second to ensure adequate temporal resolution. Droplet impact was recorded using a Phantom V710 high-speed camera with the Navitar 12× lens. For spreading events, recording was done at 37,000 fps and at 26,000 fps for splashing. Under shadowgraph mode, image resolutions were in the range of 82 to 132 pixels/mm at an exposure time of 3-4 μs. Our shadowgraph setups were backlit, through a Thorlabs-engineered diffuser, by a Photofluor II lamp.

2.5. Image analysis

For the dripping experiments, a custom MATLAB script was employed to obtain the minimum filament (neck) diameter. The script first converts all the images to grayscale and then binarizes them to enhance feature detection. It then employs a boundary detection algorithm, resulting in two edge profiles. The minimum filament diameter is calculated as the minimum distance between these two profiles.

For the impact experiments, a custom MATLAB script was used to measure the diameter and velocity of the droplets. Similar to the dripping analysis, the script converts all images to grayscale and then binarizes them for feature detection. The code then employs boundary detection and circle-fitting algorithms to measure droplet diameters. Velocity calculations are performed by tracking the displacement between consecutive images; a linear regression on the displacements calculates the average velocities. For contact angle analysis, the script detects the droplet boundary and the pinning points on both sides of the droplet. The distance between these two points provides the spreading diameter, which is then made dimensionless by the diameter of the droplets in flight, D_0. At each contact point, a quadratic polynomial is fitted around the droplet's edge using a constrained least-squares method. This allows precise derivation of the contact angles from the tangent's angle relative to the horizontal plane. Concurrently, the contact line velocity, U_{CL}, is calculated from the change in the spreading diameter over time.

3. Result and discussions

3.1. Pinch-off

Our experimental results include snapshots of the thinning and breakup process, and report the minimum neck diameter as the droplet surface thins on its way to break up, these are for both pure liquids and nanosuspensions. The findings, shown in Fig. 2, demonstrate that the addition of stable silica nanoparticles does not alter the dynamics of breakup.

Fig. 2a shows the indistinguishable thinning and route to the breakup between the nanosuspensions and their base liquids, from the early stages of thinning to the pinch-off. Quantitatively, Fig. 2b shows the variation of the minimum neck radius as a function of the dimensionless time to the breakup, with both behaviors in agreement with the well-known inviscid dynamics [22]. Inviscid thinning is known to scale with $r \sim \tau^{2/3}$, with the potential law arising from the balance of inertial and surface tension forces [4,22]. Other thinning regimes exist, with the flow transitioning between these based on the competition of viscous, inertial, and surface tension effects and the internal dynamics within the neck [5]. It is thus important to point out that the particles within the nanosuspension do not cause changes to either the viscosity or the internal dynamics. As seen in the results, the pinch-off shapes of the loaded and unloaded fluids, Fig. 2c, overlap at all scales, including at the pinch-off point. The shape of an inviscid breakup is self-similar, with a front pinching angle of 18.1 degrees and an overturning surface resembling the region near the stalk of an apple [21]. Both, the pinching angle and the overturning are readily observed in our data, for both unloaded and loaded suspensions, Fig. 2b and c. Consequently, we conclude that the characteristic self-similar behavior of inviscid thinning is seen on both the loaded and unloaded suspensions; this indicates that the presence of stable nanoparticles has a negligible effect on the pinch-off. Example videos of the breakup of the unloaded and loaded solutions

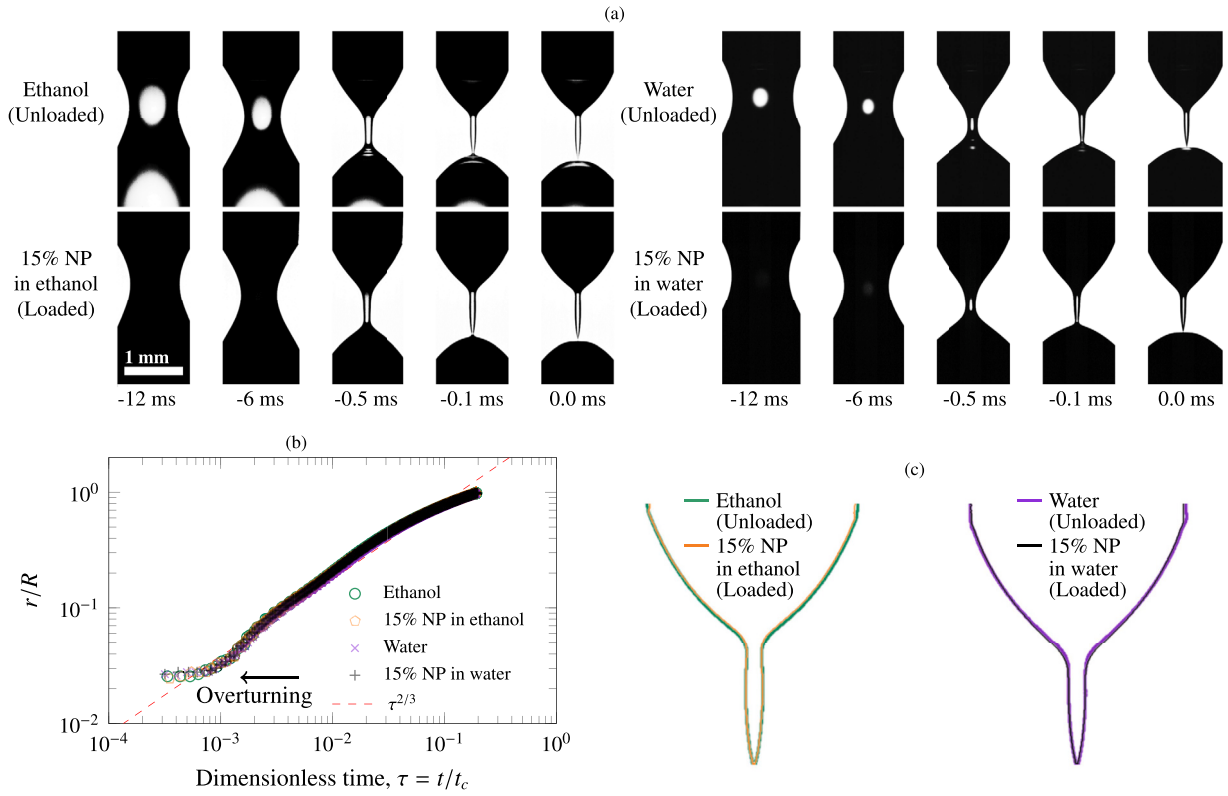

Fig. 2. Breakup experiments results for ethanol, 15 wt.% particle loaded ethanol, water, and 15 wt.% particle loaded water. (a) Snapshots of the thinning section during dripping from early stages of thinning till pinch-off. (b) Evolution of the minimum neck radius until breakup. Time is made dimensionless by dividing it by the capillary time as $\tau = t/t_c = t/\sqrt{\rho R^3/\sigma}$. (c) Overlay of the base and nanoparticle-loaded liquids contour profiles at the moment of pinch-off.

are in the Supplementary Material. Supplementary Movie 1 (UnloadedBreakup.mov) shows the typical dripping breakup behavior observed for a pendant droplet of pure ethanol, while Supplementary Movie 2 (LoadedBreakup.mov) shows the dripping breakup of an ethanol suspension containing 15 wt.% nanoparticles.

3.2. Spreading

We now examine the spreading and dynamic wetting upon impact of a droplet onto a glass substrate at an impact speed of $U_0 = 1.00 \pm 0.02$ m/s. It is known that spreading and splashing behavior depends on the liquid properties and that ethanol will splash at slower impacting speeds than water. Our studies focus on ethanol droplets with various silica nanoparticle concentrations. The spreading dimensionless diameter (d/D_0, where D_0 is the initial drop diameter before impact) in terms of the time from impact is seen in Fig. 3a. Our experiments include unloaded and loaded solutions, with particle concentrations up to 15 wt.%. Our results show that the maximum spreading diameter, across all the nanosuspension concentrations, is consistent with that of pure ethanol, i.e. $d/D_0 = 3.72 \pm 0.05$. The rate of change remains in agreement with pure ethanol, with the maximum spreading diameter consistently achieved approximately 10 ms after impact. The absence of receding, characteristic of wettable systems, across all concentrations suggests that the nanoparticles do not affect the suspension's surface tension or the dynamics of the contact line. Under these smooth spreading conditions, we also extracted the advancing dynamic contact angle (θ_D) as a function of the contact line velocity (U_{CL}), and this is seen in Fig. 3b. It has been well established that pure ethanol reaches an advancing asymptotic contact angle $\theta_D = 98 \pm 3$ degrees [48], at a contact line velocity of 2.00 ± 0.02 m/s. This asymptotic value remains consistent across all the nanosuspension concentrations. At low contact line speeds ($U_{CL} < 0.5$ m/s), measurement uncertainties arise due to the dramatic change in dynamic contact angle as the rim curvature decreases rapidly. In addition, as the dynamics slow down, the contact line moves only a few pixels between frames which causes inaccuracies in calculating the spreading velocity. In Fig. 3b, we have included example error bars to illustrate these effects. As seen, variations across all nanoparticle concentrations remain within the experimental error, confirming that nanoparticles do not systematically alter the transient contact angle dynamics. Fig. 3c presents snapshots contrasting the spreading behavior of pure ethanol with the suspension at the highest nanoparticle concentration, i.e. 15 wt.% at the times from impact. Both cases achieve the same maximum spreading dimensionless diameter, with no evidence of lamella lifting or rim instabilities, indicative of smooth spreading behavior. For the spreading of water-based nanosuspensions at a 15 wt.% nanoparticle concentration and an impact velocity of $U_0 = 1.0 \pm 0.02$ m/s, our experiments demonstrate that both the dynamic contact angle and the spreading diameter are in agreement with that of pure water ($\theta_{max} = 98 \pm 2$ degrees and $d/D_0 = 2.92 \pm 0.03$); these results are shown in the Supplementary Material Fig. S3. These findings indicate that nanoparticles do not change the spreading dynamics of additive-free suspensions. Example videos of the spreading of the unloaded and loaded solutions are in the Supplementary Material. Supplementary Movie 3 (UnloadedSpreading.mov) shows the spreading behavior of a pure ethanol droplet following impact onto a solid substrate at 1 m/s while Supplementary Movie 4 (LoadedSpreading.mov) shows the spreading of an ethanol suspension containing 15 wt.% nanoparticles following impact at 1 m/s.

3.3. Splashing

At higher impact velocities, $U_0 > 2.37$ m/s, we observe the impact of ethanol droplets transitioning from spreading to splashing, which is characterized by the disintegration of the lamella into smaller droplets. The onset of splashing is governed by multiple factors, including the impact characteristics and the fluid properties, with recent models adding the influence of the surrounding gas viscosity [67], η_g and the wedge

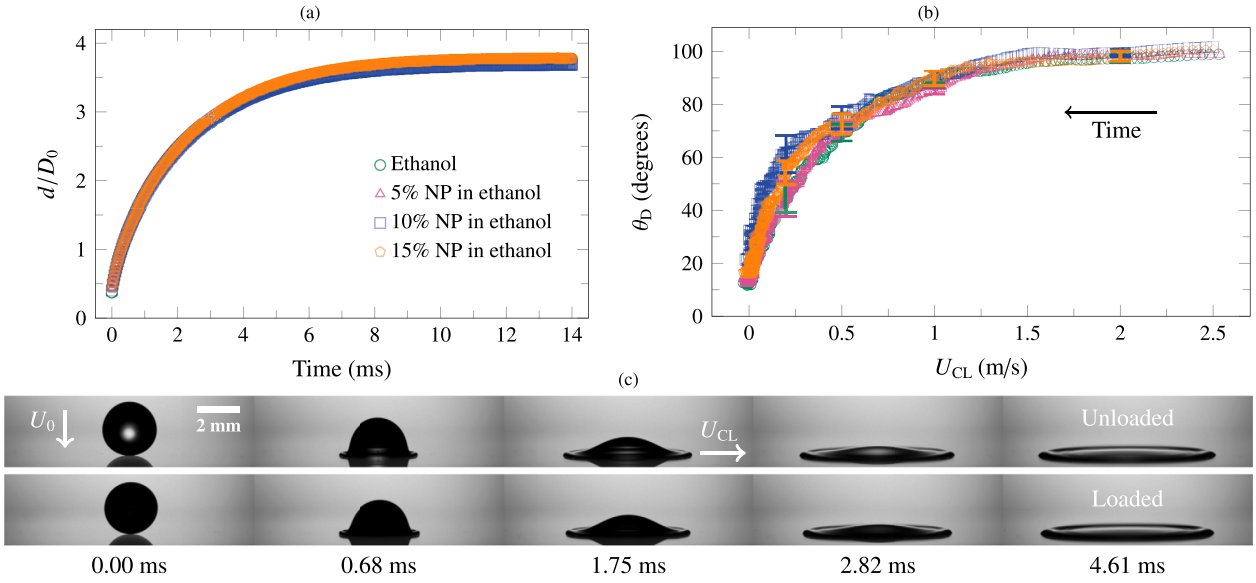

Fig. 3. Spreading dynamics for ethanol droplets with varying nanoparticle (NP) concentrations impacting on smooth glass at an impact velocity $U_0 = 1.00 \pm 0.02$ m/s. (a) Spreading dimensionless diameter (d/D_0) in terms of the time from impact; all NP concentrations exhibit similar spreading diameters at all times. (b) Dynamic contact angle in terms of the contact line velocity (U_{CL}); as seen, all NP concentrations converge to the same asymptotic value. At all conditions, variations are within experimental error, as indicated by the example error bars (at 2.0, 1.0, 0.5, and 0.2 m/s). (c) Time-sequence images comparing the spreading of ethanol droplets with (bottom, $D_0 = 2.45$ mm) and without (top, $D_0 = 2.52$ mm) 15 wt.% nanoparticles.

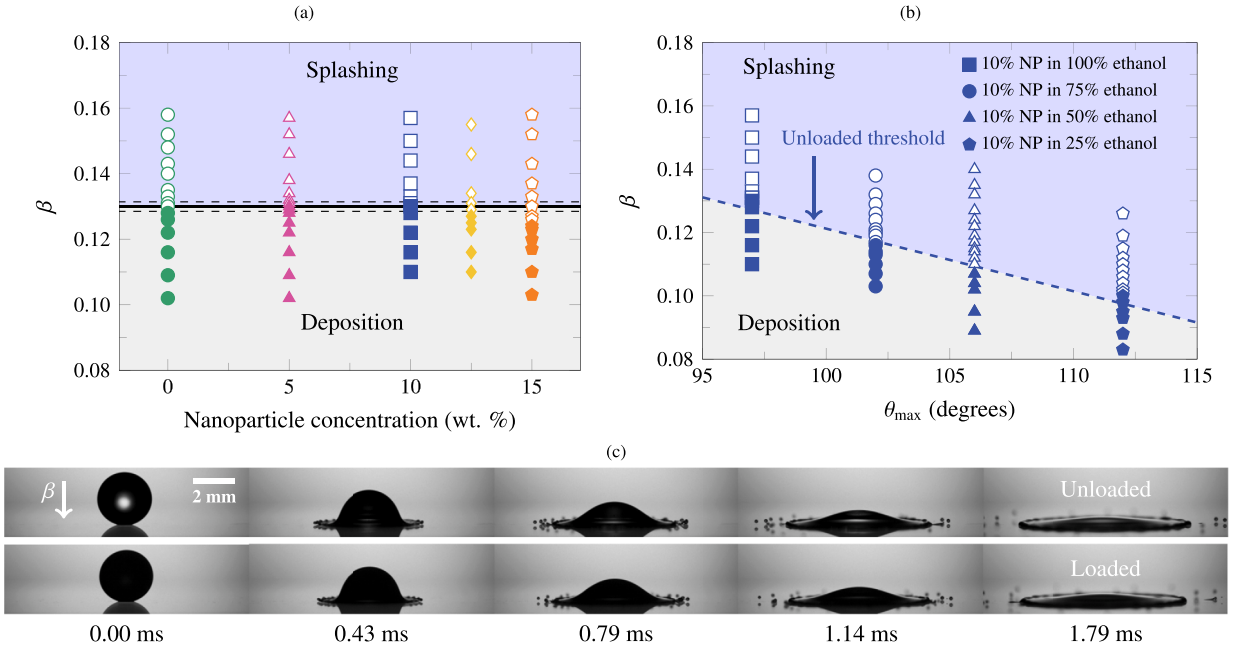

Fig. 4. Splashing dynamics on smooth glass. Open symbols represent splashing, while solid ones represent deposition (spreading). (a) Splashing behavior, in terms of the splashing ratio, of ethanol droplets with varying nanoparticle (NP) concentrations; the middle solid line shows the predicted value as calculated from past works [50,66] with the two dashed parallel lines representing the associated error due to the experimental uncertainty of the variables. (b) The splashing ratio in terms of the maximum spreading contact angle for ethanol-water mixtures, each with a 10 wt%. nanoparticle concentration. The dashed line represents the trend for mixtures with no nanoparticles. (c) Time-sequence images comparing the splashing of 50 wt%. ethanol-water droplets with (bottom, $D_0 = 2.56$ mm) and without (top, $D_0 = 2.59$ mm) 10 wt.% nanoparticles at $\beta = 0.116$.

angle, α, formed by the lamella at the moment of splashing. The splashing ratio, β, incorporates aerodynamic lubrication theory and capillary retraction forces, to predict the critical conditions for the onset of splashing [7]. For low Ohnesorge numbers (Oh $\ll$ 1) [66], the splashing condition is defined as:

$$\beta = \frac{2.22}{\tan\alpha} \cdot \frac{\eta_g^{\frac{1}{2}} \left(\rho D_0 U_0^5\right)^{\frac{1}{6}}}{\sigma^{\frac{2}{3}}}. \quad (1)$$

Recent work has demonstrated that this ratio, coupled with the maximum advancing contact angle, parameterizes the splashing behavior in terms of wettability and surface roughness [50,51]. Our analysis of the splashing dynamics begins with Fig. 4a showing the splashing ratio in terms of the nanosuspension concentration. The pure unloaded ethanol is seen in green circles, with the onset of splashing, i.e. the divide between spreading (solid symbols) and splashing (open symbols), occurring at $\beta \approx 0.1300 \pm 0.0014$ for glass, which is in agreement

with past studies [50,66]. Further to this, all the loaded suspensions splash at the same critical ratio, indicating that nanoparticles do not alter the splashing behavior. In particular, at a 15 wt.% nanoparticle concentration, the onset of splashing occurs at $U_0 = 1.81 \pm 0.02$ m/s, in agreement with the predicted value of $U_0^{predicted} = 1.85 \pm 0.02$ m/s. We note that our nanosuspensions are in the inviscid splashing regime, as $Re^{-2}Oh^{-2} - 1.21t_e^{3/2} \gg \frac{\sqrt{3}}{2}Re^{-1}t_e^{-1/2}$, where $Re = \frac{\rho D_0 U_0}{\eta}$ and t_e is the time in which the ejecta is formed, i.e. $t_e \approx 100$ μs.

We also employed nanosuspensions of ethanol and water mixtures (75 wt.%, 50 wt.%, and 25 wt.% ethanol) to investigate further the effects of particle concentration on wettability and splashing. Given the practical constraints of our experimental setup, which limited our ability to achieve the high impact velocities required for water splashing ($\gtrsim 5$ m/s), we selected ethanol and ethanol-water solutions for the splashing experiments due to their significantly lower splashing threshold. Results are shown in Fig. 4b, where all suspensions are at a 10 wt.% nanoparticle concentration. As expected, these aqueous suspensions possess different values for the surface tension, leading to having different maximum dynamic contact angles, i.e. from $\theta_{max} = 98$ degrees for the pure ethanol suspension to 112 degrees for the 25 wt.% ethanol suspension, as shown in Supplementary Material Fig. S4a. Previous studies [50], for unloaded fluids, reported that an increase in θ_{max} decreases the splashing ratio, and this behavior is in agreement with our results (Fig. 4b). The dashed line in Fig. 4b represents the predicted splashing threshold for unloaded ethanol-water mixtures, with nanosuspensions fully in agreement. This further confirms that additive-free nanoparticle suspensions, even at a 10 wt.% concentration, do not influence the splashing dynamics, or the dynamic wettability.

We note that our impacting experiments, spanning $1,384 < Re < 4,336$, were carefully conducted above and below the critical threshold to assess any significant effect of the nanoparticles on the onset of splashing. Although previous studies have suggested that splash suppression is linked to potential shear-thickening effects (undetectable by standard rheology) [61], our results indicate that, as we moved above the threshold, splashing became increasingly violent, with no signs of suppression across all concentrations and ethanol-aqueous nanosuspensions. Finally, Fig. 4c presents snapshots of the splashing dynamics for the 50 wt.% ethanol suspension with and without 10 wt.% nanoparticles at $\beta = 0.116$. Surface instabilities are already visible in both cases at 0.43 ms, and by 0.79 ms, secondary droplet formation confirms splashing. At all times, the contact line diameter remains consistent between the two cases. These findings reinforce that nanoparticles do not affect the splashing behavior. Example videos of the splashing of the unloaded and loaded solutions are in the Supplementary Material. Supplementary Movie 5 (UnloadedSplashing.mov) shows the splashing behavior of a 50% ethanol aqueous solution droplet following impact at 1.93 m/s, while Supplementary Movie 6 (LoadedSplashing.mov) shows the splashing behavior of a 50% ethanol aqueous suspension droplet containing 10 wt.% nanoparticles following impact at 1.94 m/s.

4. Conclusions

In this study, we have analyzed the dynamics of water, ethanol, and aqueous ethanol suspensions loaded, at various concentrations, with nanoparticles. Our results demonstrate that the dynamics of additive-free stable silica nanosuspensions follow the thinning, breakup, and impact dynamics of their unloaded base liquids, even at high particle concentrations (up to 15 wt.%). Previous studies have claimed that nanoparticles themselves significantly alter droplet dynamics, such as the liquid breakup [23,25,27–32,44,45,47], wetting [55–60], spreading [55–64], or the splashing [61–63]. These findings, while being essential steps in understanding nanosuspensions behavior, seem to provide contradictory conclusions. Consequently, this study resolves a key debate in particle-loaded droplet dynamics: additive-free nanoparticles do not change droplet breakup, spreading, or splashing. Our results highlight the often overlooked role of additives, surfactants, and inter-particle interactions on the droplet dynamics. Past works have found that surfactants alone modify the thinning [68] and splashing behavior [51] of droplets, so it is not surprising that these, and other additives, are responsible for the differences observed in suspensions in past works.

Our findings open up new possibilities across diverse fields. For example, in inkjet printing and spray coating, our findings imply that by using well-disperse additive-free particles, the jetting of highly loaded ink can be achieved without altering the liquid properties and the jetting parameters. Other fields such as drug delivery, microfluidics, and additive manufacturing, where Newtonian-like flows are well understood, can benefit from our findings by facilitating the effective transport of dense nanosuspensions.

Future work can build on our results and test alternative methods to produce additive-free stable nanosuspensions, as well as focus on other particle sizes, shapes, and surface properties. In particular, industrially scalable methods would be of great interest for inkjet and spray technologies.

CRediT authorship contribution statement

Mete Abbot: Writing – original draft, Visualization, Validation, Methodology, Investigation, Formal analysis, Data curation, Conceptualization. **Muhammad Hamza Iqbal:** Writing – review & editing, Writing – original draft, Visualization, Validation, Methodology, Investigation, Formal analysis, Data curation, Conceptualization. **Lingyue Liu:** Writing – original draft, Methodology. **Erin Koos:** Writing – review & editing, Supervision, Conceptualization. **Ilia V. Roisman:** Writing – review & editing, Supervision, Conceptualization. **Jeanette Hussong:** Writing – review & editing, Supervision, Conceptualization. **Alfonso Arturo Castrejón-Pita:** Writing – review & editing, Supervision, Conceptualization. **José Rafael Castrejón-Pita:** Writing – review & editing, Writing – original draft, Supervision, Conceptualization.

Declaration of generative AI and AI-assisted technologies in the writing process

During the preparation of this work, the author(s) used Google Gemini for minor language suggestions and refinements. After using this tool/service, the authors reviewed and edited the content as needed and take full responsibility for the content of the publication.

Declaration of competing interest

The authors declare the following financial interests/personal relationships which may be considered as potential competing interests: J.R. Castrejon-Pita reports financial support was provided by the Engineering and Physical Sciences Research Council through UCL's 2022-25 Impact Acceleration Account. A.A. Castrejon-Pita reports financial support was provided by the Engineering and Physical Sciences Research Council through the grant EP/W016036/1. M. Abbot reports financial support was provided by the European Union through grant 955612. J.R. Castrejon-Pita reports financial support was provided by InnovateUK through the KTP grant 10019184. If there are other authors, they declare that they have no known competing financial interests or personal relationships that could have appeared to influence the work reported in this paper.

Acknowledgements

This project has been funded by the European Union's Horizon 2020 research and innovation programme under the Marie Skłodowska-Curie grant agreement No 955612 (nanoPaInt), UCL's Engineering and Physical Sciences Research Council (EPSRC) Impact Acceleration Account 2022-25 and the US-CBET/UK-EPSRC grant EP/W016036/1. JRC-P acknowledges the support from the Knowledge Transfer Partnership

project 10019184 from InnovateUK. The authors wish to thank R. González Rubio, E. Guzmán Solís, and F. Ortega Gómez (Department of Physical Chemistry, University Complutense of Madrid) for valuable discussions and assistance with the initial nanosuspension structural and rheological characterization. We thank T. Tudlahar, from Trijet Ltd, for the assistance provided with the TriPAV viscosity measurements.

Appendix A. Supplementary material

Supplementary material related to this article can be found online at https://doi.org/10.1016/j.jcis.2025.137570.

Data availability

Data will be made available upon reasonable request to the corresponding author.

References

[1] A.L. Yarin, Drop impact dynamics: splashing, spreading, receding, bouncing..., Annu. Rev. Fluid Mech. 38 (2006) 159–192, https://doi.org/10.1146/annurev.fluid.38.050304.092144.
[2] M. Rein, Phenomena of liquid drop impact on solid and liquid surfaces, Fluid Dyn. Res. 12 (1993) 61–93, https://doi.org/10.1016/0169-5983(93)90106-K.
[3] J. Eggers, E. Villermaux, Physics of liquid jets, Rep. Prog. Phys. 71 (2008) 036601, https://doi.org/10.1088/0034-4885/71/3/036601.
[4] J. Eggers, Nonlinear dynamics and breakup of free-surface flows, Rev. Mod. Phys. 69 (1997) 865, https://doi.org/10.1103/RevModPhys.69.865.
[5] J.R. Castrejón-Pita, A.A. Castrejón-Pita, S.S. Thete, K. Sambath, I.M. Hutchings, J. Hinch, J.R. Lister, O.A. Basaran, Plethora of transitions during breakup of liquid filaments, Proc. Natl. Acad. Sci. USA 112 (2015) 4582–4587, https://doi.org/10.1073/pnas.1418541112.
[6] C. Josserand, S.T. Thoroddsen, Drop impact on a solid surface, Annu. Rev. Fluid Mech. 48 (2016) 365–391, https://doi.org/10.1146/annurev-fluid-122414-034401.
[7] G. Riboux, J.M. Gordillo, Experiments of drops impacting a smooth solid surface: a model of the critical impact speed for drop splashing, Phys. Rev. Lett. 113 (2014) 024507, https://doi.org/10.1103/PhysRevLett.113.024507.
[8] J.F. Morris, Toward a fluid mechanics of suspensions, Phys. Rev. Fluids 5 (2020) 110519, https://doi.org/10.1103/PhysRevFluids.5.110519.
[9] J.J. Stickel, R.L. Powell, Fluid mechanics and rheology of dense suspensions, Annu. Rev. Fluid Mech. 37 (2005) 129–149, https://doi.org/10.1146/annurev.fluid.36.050802.122132.
[10] A. Gans, E. Dressaire, B. Colnet, G. Saingier, M.Z. Bazant, A. Sauret, Dip-coating of suspensions, Soft Matter 15 (2019) 252–261, https://doi.org/10.1039/C8SM01785A.
[11] L. Pawlowski, Suspension and solution thermal spray coatings, Surf. Coat. Technol. 203 (2009) 2807–2829, https://doi.org/10.1016/j.surfcoat.2009.03.005.
[12] H. Yoo, C. Kim, Experimental studies on formation, spreading and drying of inkjet drop of colloidal suspensions, Colloids Surf. A, Physicochem. Eng. Asp. 468 (2015) 234–245, https://doi.org/10.1016/j.colsurfa.2014.12.032.
[13] J.R. Castrejon-Pita, W.R.S. Baxter, J. Morgan, S. Temple, G.D. Martin, I.M. Hutchings, Future, opportunities and challenges of inkjet technologies, At. Sprays 23 (2013) 541–565, https://doi.org/10.1615/AtomizSpr.2013007653.
[14] P.K. Tyagi, R. Kumar, P.K. Mondal, A review of the state-of-the-art nanofluid spray and jet impingement cooling, Phys. Fluids 32 (12) (2020), https://doi.org/10.1063/5.0033503.
[15] Y.T. Aksoy, Y. Zhu, P. Eneren, E. Koos, M.R. Vetrano, The impact of nanofluids on droplet/spray cooling of a heated surface: a critical review, Energies 14 (2020) 80, https://doi.org/10.3390/en14010080.
[16] S. Jacob, A.B. Nair, J. Shah, Emerging role of nanosuspensions in drug delivery systems, Biomater. Res. 24 (2020) 3, https://doi.org/10.1186/s40824-020-0184-8.
[17] Y. Sasson, G. Levy-Ruso, O. Toledano, I. Ishaaya, Nanosuspensions: emerging novel agrochemical formulations, in: Insecticides Design Using Advanced Technologies, Springer, 2007, pp. 1–39.
[18] J. Eggers, Universal pinching of 3D axisymmetric free-surface flow, Phys. Rev. Lett. 71 (1993) 3458, https://doi.org/10.1103/PhysRevLett.71.3458.
[19] A.U. Chen, P.K. Notz, O.A. Basaran, Computational and experimental analysis of pinch-off and scaling, Phys. Rev. Lett. 88 (2002) 174501, https://doi.org/10.1103/PhysRevLett.88.174501.
[20] I.V. Roisman, M. Abboud, P. Brockmann, F. Berner, R. Berger, P. Rothmann-Brumm, H.M. Sauer, E. Dörsam, J. Hussong, Forced flows in liquid bridges, Curr. Opin. Colloid Interface Sci. (2023) 101738, https://doi.org/10.1016/j.cocis.2023.101738.
[21] J.R. Castrejón-Pita, A.A. Castrejón-Pita, E.J. Hinch, J.R. Lister, I.M. Hutchings, Self-similar breakup of near-inviscid liquids, Phys. Rev. E 86 (2012) 015301, https://doi.org/10.1103/PhysRevE.86.015301.
[22] R.F. Day, E.J. Hinch, J.R. Lister, Self-similar capillary pinchoff of an inviscid fluid, Phys. Rev. Lett. 80 (1998) 704, https://doi.org/10.1103/PhysRevLett.80.704.
[23] W. Mathues, C. McIlroy, O.G. Harlen, C. Clasen, Capillary breakup of suspensions near pinch-off, Phys. Fluids 27 (2015) 093301, https://doi.org/10.1063/1.4930011.
[24] A.N. Alexandrou, A.V. Bazilevskii, V.M. Entov, A.N. Rozhkov, A. Sharaf, Breakup of a capillary bridge of suspensions, Fluid Dyn. 45 (2010) 952–964, https://doi.org/10.1134/S001546281006013X.
[25] C. McIlroy, O.G. Harlen, Modelling capillary break-up of particulate suspensions, Phys. Fluids 26 (2014) 033101, https://doi.org/10.1063/1.4866789.
[26] J. Zou, F. Lin, C. Ji, Capillary breakup of armored liquid filaments, Phys. Fluids 29 (2017) 062103, https://doi.org/10.1063/1.4984836.
[27] F.J. Galindo-Rosales, J.P. Segovia-Gutiérrez, F.T. Pinho, M.A. Alves, J. de Vicente, Extensional rheometry of magnetic dispersions, J. Rheol. 59 (2015) 193–209, https://doi.org/10.1122/1.4902356.
[28] R.J.E. Andrade, A.R. Jacob, F.J. Galindo-Rosales, L. Campo-Deaño, Q. Huang, O. Hassager, G. Petekidis, Dilatancy in dense suspensions of model hard-sphere-like colloids under shear and extensional flow, J. Rheol. 64 (2020) 1179–1196, https://doi.org/10.1122/1.51436531.
[29] S. Khandavalli, J.P. Rothstein, Extensional rheology of shear-thickening fumed silica nanoparticles dispersed in an aqueous polyethylene oxide solution, J. Rheol. 58 (2014) 411–431, https://doi.org/10.1122/1.4864620.
[30] C. Lang, J. Hendricks, Z. Zhang, N.K. Reddy, J.P. Rothstein, M.P. Lettinga, J. Vermant, C. Clasen, Effects of particle stiffness on the extensional rheology of model rod-like nanoparticle suspensions, Soft Matter 15 (2019) 833–841, https://doi.org/10.1039/C8SM01925H.
[31] A.W.K. Ma, F. Chinesta, T. Tuladhar, M.R. Mackley, Filament stretching of carbon nanotube suspensions, Rheol. Acta 47 (2008) 447–457, https://doi.org/10.1007/s00397-007-0247-y.
[32] H.C.-H. Ng, A. Corker, E. García-Tuñón, R.J. Poole, GO CaBER: capillary breakup and steady-shear experiments on aqueous graphene oxide (GO) suspensions, J. Rheol. 64 (2020) 81–93, https://doi.org/10.1122/1.5109016.
[33] Y. Hwang, J.-K. Lee, J.-K. Lee, Y.-M. Jeong, S. Cheong, Y.-C. Ahn, S.H. Kim, Production and dispersion stability of nanoparticles in nanofluids, Powder Technol. 186 (2008) 145–153, https://doi.org/10.1016/j.powtec.2007.11.020.
[34] S. Verma, S. Kumar, R. Gokhale, D.J. Burgess, Physical stability of nanosuspensions: investigation of the role of stabilizers on Ostwald ripening, Int. J. Pharm. 406 (2011) 145–152, https://doi.org/10.1016/j.ijpharm.2010.12.027.
[35] S. Al-Anssari, M. Arif, S. Wang, A. Barifcani, S. Iglauer, Stabilising nanofluids in saline environments, J. Colloid Interface Sci. 508 (2017) 222–229, https://doi.org/10.1016/j.jcis.2017.08.043.
[36] X.-J. Wang, X.-F. Li, S. Yang, Influence of pH and SDBS on the stability and thermal conductivity of nanofluids, Energy Fuels 23 (2009) 2684–2689, https://doi.org/10.1021/ef800865a.
[37] S. Chakraborty, P.K. Panigrahi, Stability of nanofluid: a review, Appl. Therm. Eng. 174 (2020) 115259, https://doi.org/10.1016/j.applthermaleng.2020.115259.
[38] S. Bindgen, F. Bossler, J. Allard, E. Koos, Connecting particle clustering and rheology in attractive particle networks, Soft Matter 16 (2020) 8380–8393, https://doi.org/10.1039/D0SM00861C.
[39] W. Stöber, A. Fink, E. Bohn, Controlled growth of monodisperse silica spheres in the micron size range, J. Colloid Interface Sci. 26 (1968) 62–69, https://doi.org/10.1016/0021-9797(68)90272-5.
[40] A. d, S. da Silva, J.H.Z. Dos Santos, Stöber method and its nuances over the years, Adv. Colloid Interface Sci. 314 (2023) 102888, https://doi.org/10.1016/j.cis.2023.102888.
[41] P. Drašar, The sol-gel handbook: Synthesis, characterization and applications, David Levy, Marcos Zayat (Eds.), Chem. Listy 110 (3) (2016) 229–230, https://doi.org/10.1002/9783527670819.
[42] G.H. McKinley, A. Tripathi, How to extract the Newtonian viscosity from capillary breakup measurements in a filament rheometer, J. Rheol. 44 (2000) 653–670, https://doi.org/10.1122/1.551105.
[43] D.C. Vadillo, T.R. Tuladhar, A.C. Mulji, S. Jung, S.D. Hoath, M.R. Mackley, Evaluation of the inkjet fluid's performance using the "Cambridge Trimaster" filament stretch and break-up device, J. Rheol. 54 (2010) 261–282, https://doi.org/10.1122/1.3302451.
[44] J.H. García-Ortiz, F.J. Galindo-Rosales, Extensional magnetorheology as a tool for optimizing the formulation of ferrofluids in oil-spill clean-up processes, Processes 8 (2020) 597, https://doi.org/10.3390/pr8050597.
[45] J.M. Nunes, F.J. Galindo-Rosales, L. Campo-Deaño, Extensional magnetorheology of viscoelastic human blood analogues loaded with magnetic particles, Materials 14 (2021) 6930, https://doi.org/10.3390/ma14226930.
[46] E. Di Giuseppe, A. Davaille, E. Mittelstaedt, M. François, Rheological and mechanical properties of silica colloids: from Newtonian liquid to brittle behaviour, Rheol. Acta 51 (2012) 451–465, https://doi.org/10.1007/s00397-011-0611-9.
[47] H. Kitching, M.J. Shiers, A.J. Kenyon, I.P. Parkin, Self-assembly of metallic nanoparticles into one-dimensional arrays, J. Mater. Chem. A 1 (2013) 6985–6999, https://doi.org/10.1039/C3TA00089C.
[48] M.A. Quetzeri-Santiago, A.A. Castrejón-Pita, J.R. Castrejón-Pita, The effect of surface roughness on the contact line and splashing dynamics of impacting droplets, Sci. Rep. 9 (2019) 15030, https://doi.org/10.1038/s41598-019-51490-5.
[49] C.J. Howland, A. Antkowiak, J.R. Castrejón-Pita, S.D. Howison, J.M. Oliver, R.W. Style, A.A. Castrejón-Pita, It's Harder to splash on soft solids, Phys. Rev. Lett. 117 (2016) 184502, https://doi.org/10.1103/PhysRevLett.117.184502.

[50] M.A. Quetzeri-Santiago, K. Yokoi, A.A. Castrejón-Pita, J.R. Castrejón-Pita, Role of the dynamic contact angle on splashing, Phys. Rev. Lett. 122 (2019) 228001, https://doi.org/10.1103/PhysRevLett.122.228001.
[51] N. Varghese, T.C. Sykes, M.A. Quetzeri-Santiago, A.A. Castrejón-Pita, J.R. Castrejón-Pita, Effect of surfactants on the splashing dynamics of drops impacting smooth substrates, Langmuir 40 (2024) 8781–8790, https://doi.org/10.1021/acs.langmuir.3c03248.
[52] E.J. Vega, A.A. Castrejón-Pita, Suppressing prompt splash with polymer additives, Exp. Fluids 58 (2017) 57, https://doi.org/10.1007/s00348-017-2341-y.
[53] A.L. Yarin, D.A. Weiss, Impact of drops on solid surfaces: self-similar capillary waves, and splashing as a new type of kinematic discontinuity, J. Fluid Mech. 283 (1995) 141–173, https://doi.org/10.1017/S0022112095002266.
[54] I.V. Roisman, Inertia dominated drop collisions. II. An analytical solution of the Navier-Stokes equations for a spreading viscous film, Phys. Fluids 21 (2009) 052104, https://doi.org/10.1063/1.3129283.
[55] S. Vafaei, T. Borca-Tasciuc, M.Z. Podowski, A. Purkayastha, G. Ramanath, P.M. Ajayan, Effect of nanoparticles on sessile droplet contact angle, Nanotechnology 17 (2006) 2523, https://doi.org/10.1088/0957-4484/17/10/014.
[56] A.M. Munshi, V.N. Singh, M. Kumar, J.P. Singh, Effect of nanoparticle size on sessile droplet contact angle, J. Appl. Phys. 103 (2008), https://doi.org/10.1063/1.2912464.
[57] J.T. Cieśliński, K.A. Krygier, Sessile droplet contact angle of water–Al2O3, water–TiO2 and water–Cu nanofluids, Exp. Therm. Fluid Sci. 59 (2014) 258–263, https://doi.org/10.1016/j.expthermflusci.2014.06.004.
[58] M. Hu, J. Zhou, Y. Li, X. Zhuo, D. Jing, Effects of the surface wettability of nanoparticles on the impact dynamics of droplets, Chem. Eng. Sci. 246 (2021) 116977, https://doi.org/10.1016/j.ces.2021.116977.
[59] G. Lu, Y.-Y. Duan, X.-D. Wang, Experimental study on the dynamic wetting of dilute nanofluids, Colloids Surf. A 486 (2015) 6–13, https://doi.org/10.1016/j.colsurfa.2015.09.009.
[60] S. Fusco, L. Liu, M.Á. Cabrerizo-Vílchez, E. Koos, M.Á. Rodríguez-Valverde, Vibration-triggered spreading of nanofluid drops, Phys. Fluids 36 (2024) 052014, https://doi.org/10.1063/5.0205785.
[61] M.-J. Thoraval, J. Schubert, S. Karpitschka, M. Chanana, F. Boyer, E. Sandoval-Naval, J.F. Dijksman, J.H. Snoeijer, D. Lohse, Nanoscopic interactions of colloidal particles can suppress millimetre drop splashing, Soft Matter 17 (2021) 5116–5121, https://doi.org/10.1039/D0SM01367F.
[62] Y.T. Aksoy, L. Liu, M. Abboud, M.R. Vetrano, E. Koos, Role of nanoparticles in nanofluid droplet impact on solid surfaces, Langmuir 39 (2022) 12–19, https://doi.org/10.1021/acs.langmuir.2c02578.
[63] Y.T. Aksoy, P. Eneren, E. Koos, M.R. Vetrano, Spreading-splashing transition of nanofluid droplets on a smooth flat surface, J. Colloid Interface Sci. 606 (2022) 434–443, https://doi.org/10.1016/j.jcis.2021.07.157.
[64] Z. Liu, S. Li, X. Pan, H. Fang, Mechanism study on spreading dynamics of nanofluids droplet coupled with thermal evaporation, Int. J. Heat Mass Transf. 183 (2022) 122172, https://doi.org/10.1016/j.ijheatmasstransfer.2021.122172.
[65] R. Javed, M. Zia, S. Naz, S.O. Aisida, N.U. Ain, Q. Ao, Role of capping agents in the application of nanoparticles in biomedicine and environmental remediation: recent trends and future prospects, J. Nanobiotechnol. 18 (2020) 1–15, https://doi.org/10.1186/s12951-020-00704-4.
[66] T.C. De Goede, N. Laan, K.G. De Bruin, D. Bonn, Effect of wetting on drop splashing of Newtonian fluids and blood, Langmuir 34 (2017) 5163–5168, https://doi.org/10.1021/acs.langmuir.7b03355.
[67] L. Xu, W.W. Zhang, S.R. Nagel, Drop splashing on a dry smooth surface, Phys. Rev. Lett. 94 (2005) 184505, https://doi.org/10.1103/PhysRevLett.94.184505.
[68] P.M. Kamat, B.W. Wagoner, A.A. Castrejón-Pita, J.R. Castrejón-Pita, C.R. Anthony, O.A. Basaran, Surfactant-driven escape from endpinching during contraction of nearly inviscid filaments, J. Fluid Mech. 899 (2020) A28, https://doi.org/10.1017/jfm.2020.476.